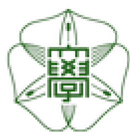
HOKKAIDO UNIVERSITY

Title	On the origin of interface states at oxide/III-nitride heterojunction interfaces
Author(s)	Matys, M.; Adamowicz, B.; Domanowska, A.; Michalewicz, A.; Stoklas, R.; Akazawa, M.; Yatabe, Z.; Hashizume, T.
Citation	Journal of Applied Physics, 120(22), 225305 https://doi.org/10.1063/1.4971409
Issue Date	2016-12-14
Doc URL	http://hdl.handle.net/2115/67847
Rights	The following article appeared in Journal of Applied Physics 120, 225305 (2016) and may be found at http://aip.scitation.org/doi/10.1063/1.4971409.
Type	article
File Information	2E4971409.pdf

Instructions for use

Hokkaido University Collection of Scholarly and Academic Papers : HUSCAP

.

On the origin of interface states at oxide/III-nitride heterojunction interfaces

M. Matys, B. Adamowicz, A. Domanowska, A. Michalewicz, R. Stoklas, M. Akazawa, Z. Yatabe, and T. Hashizume

Citation: Journal of Applied Physics **120**, 225305 (2016); doi: 10.1063/1.4971409
View online: http://dx.doi.org/10.1063/1.4971409
View Table of Contents: http://aip.scitation.org/toc/jap/120/22
Published by the American Institute of Physics

Articles you may be interested in

Mechanism of yellow luminescence in GaN at room temperature
Journal of Applied Physics **121**, 065104065104 (2017); 10.1063/1.4975116

Intragrain charge transport in kesterite thin films—Limits arising from carrier localization
Journal of Applied Physics **120**, 175302175302 (2016); 10.1063/1.4965868

Low-temperature atomic layer deposition-grown Al2O3 gate dielectric for GaN/AlGaN/GaN MOS HEMTs: Impact of deposition conditions on interface state density
Journal of Applied Physics **35**, 01A10701A107 (2016); 10.1116/1.4972870

Evolution of planar defects during homoepitaxial growth of β-Ga2O3 layers on (100) substrates—A quantitative model
Journal of Applied Physics **120**, 225308225308 (2016); 10.1063/1.4971957

AIP Publishing HORIZONS
Small Conferences. BIG Ideas.
Applied Physics Reviews
SAVE THE DATE!
3D Bioprinting: Physical and Chemical Processes
May 2–3, 2017 • Winston Salem, NC, USA

JOURNAL OF APPLIED PHYSICS **120**, 225305 (2016)

On the origin of interface states at oxide/III-nitride heterojunction interfaces

M. Matys,[1,2,a)] B. Adamowicz,[1] A. Domanowska,[2] A. Michalewicz,[2] R. Stoklas,[1,3]
M. Akazawa,[4] Z. Yatabe,[4] and T. Hashizume[1]
[1]*Research Center for Integrated Quantum Electronics, Hokkaido University, Kita-13 Nishi-8, Kita-ku, 060-8628 Sapporo, Japan*
[2]*Surface Physics and Nanostructures Dept., Institute of Physics—CSE, Silesian University of Technology, Konarskiego 22B, 44 -100 Gliwice, Poland*
[3]*Institute of Electrical Engineering, Slovak Academy of Sciences, Dubravska cesta 9, 841 04 Bratislava, Slovak Republic*
[4]*Priority Organization for Innovation and Excellence, Kumamoto University, Kumamoto 860-8555, Japan*

(Received 28 September 2016; accepted 21 November 2016; published online 14 December 2016)

The energy spectrum of interface state density, $D_{it}(E)$, was determined at oxide/III-N heterojunction interfaces in the entire band gap, using two complementary photo-electric methods: (i) photo-assisted capacitance-voltage technique for the states distributed near the midgap and the conduction band (CB) and (ii) light intensity dependent photo-capacitance method for the states close to the valence band (VB). In addition, the Auger electron spectroscopy profiling was applied for the characterization of chemical composition of the interface region with the emphasis on carbon impurities, which can be responsible for the interface state creation. The studies were performed for the AlGaN/GaN metal-insulator-semiconductor heterostructures (MISH) with Al_2O_3 and SiO_2 dielectric films and Al_xGa_{1-x} layers with x varying from 0.15 to 0.4 as well as for an Al_2O_3/InAlN/GaN MISH structure. For all structures, it was found that: (i) $D_{it}(E)$ is an U-shaped continuum increasing from the midgap towards the CB and VB edges and (ii) interface states near the VB exhibit donor-like character. Furthermore, $D_{it}(E)$ for SiO_2/Al_xGa_{1-x}/GaN structures increased with rising x. It was also revealed that carbon impurities are not present in the oxide/III-N interface region, which indicates that probably the interface states are not related to carbon, as previously reported. Finally, it was proven that the obtained $D_{it}(E)$ spectrum can be well fitted using a formula predicted by the disorder induced gap state model. This is an indication that the interface states at oxide/III-N interfaces can originate from the structural disorder of the interfacial region. Furthermore, at the oxide/barrier interface we revealed the presence of the positive fixed charge (Q_F) which is not related to $D_{it}(E)$ and which almost compensates the negative polarization charge (Q^-_{pol}). *Published by AIP Publishing.* [http://dx.doi.org/10.1063/1.4971409]

I. INTRODUCTION

AlGaN and InAlN/GaN high electron mobility transistors (HEMTs) exceed Si based devices in high voltage and high frequency microelectronics due to advantageous physical properties of nitride semiconductors, like their wide band gaps and durability at high temperatures.[1–8] It was also well established that GaN-HEMTs with an insulated gate (IG) exhibit supremacy over Schottky-gate-based ones because of the lower gate leakage current, higher breakdown voltage, better thermal stability of the gate, and mitigation of current collapse.[8–12] The Al_2O_3 and SiO_2 IG structures are particularly attractive for the application to GaN-HEMTs because of their favorable properties, i.e., the large conduction band (CB) offset at the insulator/semiconductor interfaces.[13–15] However, the electronic states existing at such interfaces may significantly influence the device performance due to uncontrolled interface charging.[16–23]

Despite the high importance of interface states at dielectric/III-N heterojunction interfaces, their origin and properties, in particular, the density distribution vs. energy, $D_{it}(E)$, in the wide band gap, E_G, and charge type (donor-like or acceptor-like) are still not clarified. The main reason of such a situation are the extreme obstacles in the quantitative characterization of interface states by means of the electrical methods in the case of III-N heterojunction based devices because of the presence of two interfaces and very long time constants for charge emission from the deep states at room temperature (RT).[11,14] It should be highlighted that solution of the above problems is a key issue to further progress in GaN-based HEMTs technology.

In the present paper, we studied the interface states at oxide/III-N heterojunction interfaces using AlGaN/GaN metal-insulator-semiconductor heterostructures (MISHs) with Al_2O_3 and SiO_2 films as insulator and $Al_xGa_{1-x}N$ layers with an Al content varying over a wide range (x) from 0.15 to 0.4 as well as an Al_2O_3/InAlN/GaN MISH structure. In this order, we applied different photo-electrical methods, which are based on the measurements of: (i) dependencies of the threshold voltage shift ($\triangle V_{th}$) in a capacitance-voltage (C-V) curves vs. temperature (T) and vs. excitation photon energy ($h\nu$ lower than EG of GaN) and (ii) photocapacitance (ΔC) vs. light intensity (Φ) with $h\nu$ larger than E_G. Such an approach allows to determine $D_{it}(E)$ spectrum of the interface

[a)]matys@rciqe.hokudai.ac.jp

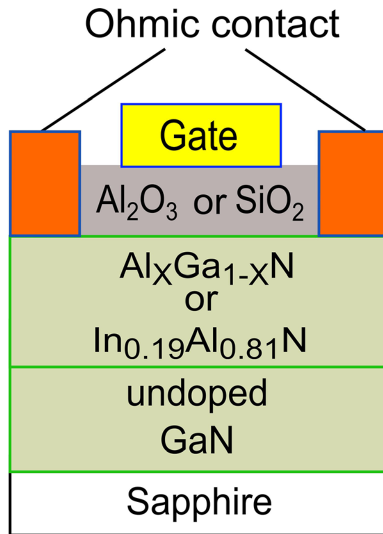

FIG. 1. Scheme of the cross-section of examined MISH structures.

states in the entire bandgap, in particular, near the valence band (VB), which is extremely difficult to achieve electrically. In addition, we characterized the chemical composition of the interface region using the Auger electron spectroscopy (AES) combined with ion sputtering, in order to identify impurities, which can be responsible for the interface states. Finally, based on the obtained results, we discussed the properties of $D_{it}(E)$ and oxide/barrier interface charges.

II. SAMPLE STRUCTURE AND FABRICATION PROCESS

In Fig. 1, we present a scheme of the studied MISH structures, i.e.:

- $Al_2O_3/Al_{0.2}Ga_{0.8}N/GaN$ with a metalorganic chemical vapor deposition (MOCVD) grown AlGaN layer (34 nm thick);
- $Al_2O_3/In_{0.19}Al_{0.81}N/GaN$ with a metalorganic vapor-phase epitaxy (MOVPE) grown InAlN layer (12 nm);

The investigated heterostructures were passivated using the two-step process:[24–28] (1) covered by a SiN (10 nm) protection film deposited by electron cyclotron resonance chemical vapor deposition (ECR CVD) to avoid damages of semiconductor surfaces during ohmic contact annealing and (2) after removal of the SiN film, covered with an Al_2O_3 layer (20 nm) deposited by atomic layer deposition (ALD)

- $SiO_2/Al_xGa_{1-x}N/GaN$ with modulation doped AlGaN layers (x = 0.15, 0.26, 0.40; 25 nm thick); SiO_2 passivation layers (22 nm) were deposited by ECR CVD.[15]

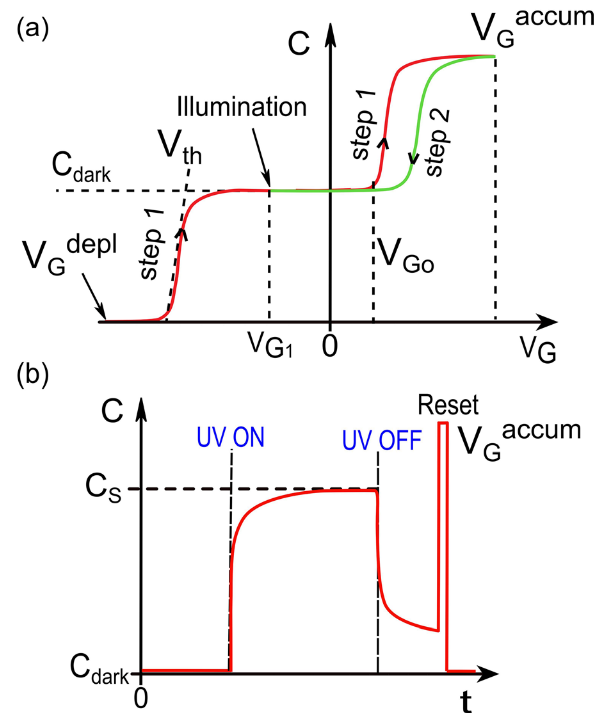

FIG. 2. Schematic illustration of the photocapacitance (ΔC) measurements.

The electric contacts were formed as follows: (1) ohmic contacts were ring-shaped Ti/Al/Ti/Au multilayers and (2) gate contacts were Al/Au or Ni/Au circles with diameters from 200 to 500 μm. All the heterojunctions were grown on a sapphire substrate and cleaned with a HF solution before passivation. The basic parameters of the examined structures, i.e., the insulator (d_I) and barrier (d_B) thicknesses, two-dimensional (2DEG) gas density (n_{2D}), carrier mobility (μ), and the sheet resistance (R_0), are summarized in Table I. The details of the sample fabrication process were reported in Refs. 11, 13, 14, 25, and 27.

III. EXPERIMENT

The ΔC characteristics vs. Φ were obtained at 1 MHZ using an impedance analyzer at RT. As a light source, a xenon lamp and band-pass filters (the light wavelength between 250 and 300 nm) were applied and Φ was changed from 10^{10} to 10^{15} photon/(cm^2 s). The value of Φ incident on the insulator surface was estimated by taking into account the effect of light reflection and transmission through a metal gate stack. We measured ΔC in the following manner (Fig. 2). First, we swept the gate voltage from depletion (V_G^{depl}) to accumulation

TABLE I. Basic structural and electrical parameters of the investigated samples at 300 K. Parameters d_I, d_B, n_{2D}, μ, and R_0 described in Sec. II; V_G^{depl}, V_{th}, V_{Go}, V_G^{accum} described in Sec. III and marked in Fig. 2.

Sample	Barrier	d_B (nm)	d_I (nm)	n_{2D} (q/cm^2)	μ (cm^2/V s)	R_0 (Ω/sq)	V_G^{depl} (V)	V_{th} (V)	V_{Go} (V)	V_G^{accum} (V)
1	$Al_{0.2}Ga_{0.8}N$	34	Al_2O_3 (20)	9.1×10^{12}	1750	500	−11.0	−8.2	1.2	5.0
3	$In_{0.19}Al_{0.81}N$	12	Al_2O_3 (20)	2.3×10^{13}	1100	287	−11.0	−8.8	2.2	5.0
4	$Al_{0.15}Ga_{0.85}N$	25	SiO_2 (22)	5.4×10^{12}	…	…	−20.0	−17.1	1.4	6.0
5	$Al_{0.26}Ga_{0.74}N$	25	SiO_2 (22)	9.8×10^{12}	…	…	−20.0	−14.4	$\gtrsim 1.5$	6.0
6	$Al_{0.40}Ga_{0.60}N$	25	SiO_2 (22)	1.8×10^{13}	…	…	−12.0	−7.8	$\gtrsim 2$	6.0

(V_G^{accum}), in order to fill the interface states with electrons (Fig. 2(a), step 1). Subsequently, we swept the gate voltage from V_G^{accum} to V_{G1} (Fig. 2(a), step 2), for which the total structure capacitance in the dark (C_{dark}) included both the dielectric (C_{ox}) and barrier layer capacitance (C_B). Keeping the bias at V_{G1}, we turned on the light. Upon illumination, we observed variations of the capacitance (C) with time (t) (Fig. 2(b)). When the C signal reached the steady-state value (C_S), we turned off the light. In order to achieve the initial state, we applied V_G^{accum} to induce accumulation. ΔC was calculated as the difference between C_S and C_{dark}. This process was repeated at different Φ, and on this basis, we determined the Φ-dependence of ΔC. The details of the measurement process can be found elsewhere.[18,19] The values of V_G^{accum} and V_G^{depl} for the examined structures are shown in Table I. Furthermore, in Table I we summarized the values of the spillover-voltage (V_{Go}) (where 2DEG electrons spill over the barrier accumulating at the oxide/barrier interface) and the threshold voltage (V_{th}) in C-V curves. The full sets of the C-V characteristics of the studied structures can be found in our recent paper.[29]

The photo-assisted C-V characteristics vs. $h\nu$ were measured at 1 MHZ by an impedance analyzer at different temperatures. As a light source, a xenon lamp and band-pass filters were applied. At the beginning, before illumination, we swept the gate voltage from $V_G = 0$ V to V_G^{accum} and then back to depletion in order to obtain the dark reference V_{th}. Next, we swept the gate voltage from V_G^{depl} to V_G^{accum} and held the structure at V_G^{accum} for 2 min to fill the interface states with electrons. At last, we swept the gate voltage from V_G^{accum} to $V_G = 0$ V and kept this bias during a period (t_{emit}) of about 1 h. After this time, we illuminated the structure for about 10 min and subsequently, in the dark conditions, we swept the gate voltage towards V_G^{depl}. Due to illumination, we observed a parallel C-V curve shift towards negative gate voltages. The $\triangle V_{th}$ in C-V characteristics was calculated as the difference between V_{th} after and before illumination. The above procedure was repeated at different T and for various $h\nu$ in order to obtain $h\nu$ and T-dependence of $\triangle V_{th}$.

For AES measurements, we used a Perkin-Elmer PHI 670 Scanning Auger Microprobe. The ion sputtering was performed with a differentially pumped scanning Ar^+ ion gun. The ion energy was 500 eV, incident angle was 60°, and the pressure during sputtering was 5×10^{-9} Torr. The low ion energy allowed to reduce the negative artifacts induced by sputtering, i.e., atom mixing and chemical reactions. The sputtered raster area was $1 \times 1\,\mathrm{mm}^2$. After each sputtering cycle (duration of 2–3 min), the AES spectrum was recorded using the primary electron beam with energy of 10 eV, which was inclined to the surface normal at an angle of about 30°. The sample current was 10 nA.

IV. ESTIMATION OF D_{it} NEAR THE VALENCE BAND FROM ΔC MEASUREMENTS

A. Model of illuminated MISH structure

The calculations of ΔC for MISH structures were performed using the following model (Fig. 3). Under illumination by photons with $h\nu$ above E_G of the barrier layer, the

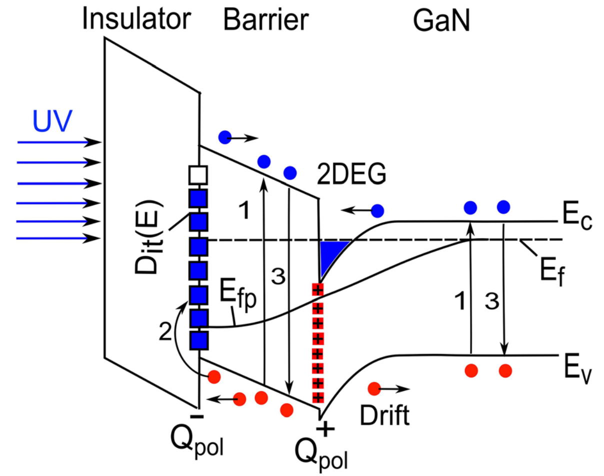

FIG. 3. Model of a MISH structure illuminated by ultraviolet (UV) light, (1) electron-hole generation in the barrier and GaN layers, (2) hole capturing by the interface states, and (3) band-to-band recombination. E_{fp} is the hole quasi-Fermi level. $Q_{pol}{}^-$ and $Q_{pol}{}^+$ means the polarization charges at insulator/barrier and barrier/GaN interfaces, respectively.

electron-hole pairs are generated both in the barrier and GaN layers at a rate $G(x)$ (where x is the distance from the insulator/barrier interface, Fig. 3), which exponentially decays according to the Lambert-Beer law. We consider the situation when the MISH structure is biased by $V_{th} < V_G < V_{Go}$. In this case, the photo- holes in the barrier layer are repelled from the barrier/GaN interface by the positive polarization charge (Q_{pol}^+) (originating from the spontaneous and piezoelectric polarization) and attracted to the insulator/barrier interface by V_G, whereas electrons are repelled from the insulator/barrier interface by V_G and attracted to the barrier/GaN interface by $Q_{pol}{}^+$. At the same time, electrons in GaN are attracted to the barrier/GaN interface by $Q_{pol}{}^+$, whereas photo-holes are repelled by this charge. The excess holes in the barrier layer are collected near the insulator/barrier interface and subsequently are captured by the interface states changing their occupation. It should be noted that due to the negligible electron concentration (n) at the insulator/barrier interface, the non-radiative recombination through the interface states is totally reduced.[18,19] However, the excess carriers can recombine radiatively through band-to-band transitions with a rate Bnp (where B is the band-to-band recombination coefficient and p is the photo-hole concentration) and non-radiatively through defects by the Shockley-Read-Hall (SRH) mechanism[30] at a rate U_{SRH}.

The model equations are based on the 1D Poisson's equation and current continuity equations in a semiconductor layer and Laplace's equation in the insulator layer. In the calculations, we assumed that the generation rate decreases exponentially versus the distance from the interface. We also considered the main bulk recombination channels, i.e., radiative band-to-band recombination and SRH recombination. The model equations were solved self-consistently using the finite element method with the following boundary conditions: (i) Neumann type boundary conditions at the insulator/barrier interface determined by the density of the interface state charge (Q_{it}) and at the barrier/GaN interface determined by $Q_{pol}{}^+$ and (ii) Dirichlet type boundary conditions at the

contacts. In particular, the boundary conditions at the insulator/barrier interface are expressed as

$$\epsilon_0\epsilon_B E_B - \epsilon_0\epsilon_I E_I = Q_{it} + Q_{fnet}, \tag{1}$$

where E_B and E_I are the electric field intensities of the barrier layer and insulator, respectively, ϵ_B and ϵ_I are the relative barrier and insulator permittivity, respectively, Q_{fnet} is the net fixed charge at the insulator/barrier interface including the negative polarization charge ($Q_{pol}{}^{-}$) and other fixed charges (Q_F) and $Q_{fnet} = Q_{pol}{}^{-} + Q_F$ ($Q_{pol}^{-} = -Q_{pol}^{+}$). Q_{it} can be expressed as follows:

$$Q_{it} = \int_{E_V}^{E_{CNL}} D_{it}(E)(1-f_{it})dE - \int_{E_{CNL}}^{E_C} D_{it}(E) f_{it} dE, \tag{2}$$

where E_V and E_C are the top of VB and the bottom of CB, respectively, E_{CNL} is the charge neutrality level and f_{it} is the occupation function of interface states expressed as

$$f_{it} = \frac{\sigma_n n_{I/B} + \sigma_p p_s(E)}{\sigma_n v_n\left[n_{I/B} + n_s(E)\right] + \sigma_p v_p\left[p_{I/B} + p_s(E)\right]}, \tag{3}$$

where σ_n and σ_p are the cross sections for capturing electrons and holes by interface states, respectively, v_n and v_p are the thermal velocities of electrons and holes, respectively, $n_{I/B}$ and $p_{I/B}$ are the concentrations of electrons and holes at the insulator/barrier interface, respectively, $n_s(E) = N_C \exp[(E - E_C)/(kT)]$, $p_s(E) = N_V \exp[(E_V - E)/(kT)]$, N_C, and N_V are the effective state densities in CB and VB, respectively.

From the solution of the model equations, we obtained the depth distributions of the electric potential V, n, and p. The calculations were performed for V_G and $V_G + V_{ac}$, where V_{ac} is the numerical equivalent of an ac signal. On this basis, we calculated the total charge in the whole structure for these biases, i.e., $Q(V_G)$ and $Q(V_G + V_{ac})$ and finally ΔC using the following formula:

$$\Delta C = \frac{Q(V_G) - Q(V_G + V_{ac})}{V_{ac}} - C_{dark}. \tag{4}$$

During the calculation of ΔC, we assumed that Q_{it} cannot follow the fast ac voltage signal but can follow the slow gate voltage sweep (high-frequency measurement). We also assumed the materials parameters of GaN and AlGaN from Ref. 31, E_{CNL} values from Refs. 26 and 32 (for $Al_xGa_{1-x}N$ with x = 0.4, $E_{CNL} = E_C - 1.75$ eV; x = 0.26, $E_{CNL} = E_C - 1.6$ eV and x = 0.15, $E_{CNL} = E_C - 1.4$ eV; for $In_{0.19}Al_{0.81}N$, $E_{CNL} = E_C - 2$ eV) and $\sigma_n = \sigma_p$ values obtained experimentally from our previous studies.[29]

B. ΔC of MISH structure

Since the measurements of ΔC are fundamental for the determination of $D_{it}(E)$, it was necessary to understand the photocapacitance effect in a MISH structure. In this order, we derived an approximate relationship of ΔC as a function of $p_{I/B}$, which explains the behavior of ΔC with Φ and impact of the insulator and barrier thicknesses (d_I and d_B), interface parameters (Q_{it} and Q_{fnet}) as well as bulk SRH life time (τ) on ΔC.

In general, C of the MISH structure under illumination, at the gate voltage of $V_{th} < V_G < V_{Go}$, can be written as

$$C \approx \frac{1}{\left(\frac{dQ_B}{dV}\right)^{-1} + C_{ox}{}^{-1}}, \tag{5}$$

where Q_B is the total charge in the barrier layer under illumination, expressed by the following relationship:

$$Q_B = q\int_0^{d_B} (p + N_d - n)dx, \tag{6}$$

where N_D is the concentration of ionized dopants. For low and medium Φ, we can assume that n is almost the same as in the dark; therefore, Q_B can be given as follows:

$$Q_B = q\int_0^{d_B} p dx + Q_B^{dark}, \tag{7}$$

where Q_B^{dark} is the total charge in the barrier layer in the dark. In Fig. 4, we displayed the calculated in-depth distribution of p in the MISH structure under $\Phi = 10^{15}$ photon/(cm^2 s) and $V_{th} < V_G < V_{Go}$ for different τ. It is clear that p in the barrier layer rapidly decreases from the oxide/barrier interface towards the barrier/GaN interface. On this basis, Q_B can be approximately expressed as

$$Q_B \approx q d_B p_{I/B} + Q_B^{dark}. \tag{8}$$

It should be noted that dQ_B^{dark}/dV is approximately equal to the capacitance of the barrier layer ($C_B = \epsilon_B/d_B$). Therefore, dQ_B/dV can be expressed as

$$\frac{dQ_B}{dV} = q d_B \frac{dp_{I/B}}{dV} + C_B. \tag{9}$$

Taking into account that $p_{I/B} = N_V \exp(-(E_{fp} - E_V(x))/(kT))$, where E_{fp} is the hole quasi-Fermi level, we can express $dp_{I/B}/dV$ as follows:

$$\frac{dp_{I/B}}{dV} \approx \frac{q}{kT} p_{I/B}. \tag{10}$$

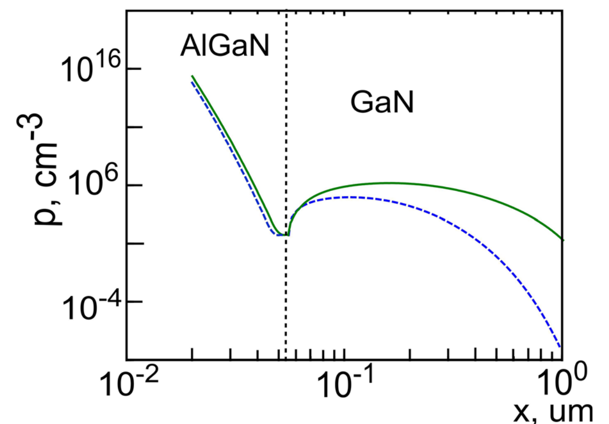

FIG. 4. Calculated depth distributions of p in the Al_2O_3/AlGaN/GaN structure with $d_I = 20$ nm, $d_B = 34$ nm under $\Phi = 10^{15}$ photon/(cm^2 s) at $V_G = -4$ V, for the ideal oxide/AlGaN interface ($Q_{it} = 0$, $Q_{fnet} = 0$). Solid line corresponds to $\tau = 10^{-7}$ s and dashed line to $\tau = 10^{-9}$ s.

Therefore, after substituting Eqs. (10) and (9) in Eq. (5), we obtain that $\Delta C = C - C_{dark}$ can be given by

$$\Delta C \approx \frac{\left(\frac{q^2 d_B}{kT} p_{I/B} + C_B\right) C_{ox}}{\frac{q^2 d_B}{kT} p_{I/B} + C_B + C_{ox}} - C_{dark}, \tag{11}$$

where $C_{dark} = \frac{C_B C_{ox}}{C_B + C_{ox}}$.

The above equation allows to understand the dependencies of ΔC vs. Φ shown in Fig. 5, which were precisely calculated using the model described in Section IV A. The simulations were performed for Al_2O_3/AlGaN/GaN structure with the different d_B and d_I in the case of the ideal Al_2O_3/AlGaN interface ($Q_{it} = 0$, $Q_{fnet} = 0$) and non-ideal interface ($Q_{it} \neq 0$, $Q_{fnet} \neq 0$), as well as for the different τ. In the calculations, we assumed $V_G = -4$ V. In particular, Eq. (11) explains well the characteristic shape of $\Delta C(\Phi)$ curves, which begin to saturate under some excitations and then approach a constant value. For example, if we take into account that $p_{I/B}$ rises monotonically with increasing Φ, we can easily find that when $p_{I/B}$ reaches the value corresponding to the condition $\frac{q^2 d_B}{kT} p_{I/B} \gg C_B + C_{ox}$, then Eq. (11) can be approximated by the relationship $\Delta C = C_{ox} - C_{dark}$. In addition, from Fig. 5 one can note that the increase of d_B caused rising of ΔC (curve 2); however, the increase of d_I resulted in lowering of ΔC (curve 3). The opposite influence of d_I and d_B can also be easily understood from Eq. (11). For example, in the case of the saturation $\Delta C = C_{ox} - C_{dark} = \frac{C_{ox}^2}{C_B + C_{ox}}$, and thus, it is evident that ΔC decreases with increasing d_I, and on the contrary, ΔC increases with increasing d_B.

Furthermore, from Fig. 5 it is evident that in the case of $Q_{it} > 0$ (donor-like states, curve 5) and $Q_{fnet} > 0$ (curve 4), the calculated dependencies of ΔC vs. Φ are shifted towards higher Φ values with respect to the ideal curve. On the contrary, the $\Delta C(\Phi)$ dependencies obtained for $Q_{it} < 0$ (acceptor-like states, curve 7) and $Q_{fnet} < 0$ (curve 6) are shifted towards lower Φ. It should be also noticed that Q_{fnet} causes parallel shifts of $\Delta C(\Phi)$ curves from the ideal one, whereas Q_{it} induces non-parallel shifts. These opposite shifts of $\Delta C(\Phi)$ curves can be easily understood in terms of Eq. (11). Namely, in the case of $Q_{fnet} > 0$, at a given Φ, $p_{I/B}$ is much lower than in the ideal case (due to repelling the free holes from the oxide/barrier interface by the positive Q_{fnet}). As a consequence, according to Eq. (11), for $Q_{fnet} > 0$, at a given Φ, ΔC is much lower than in ideal conditions, which leads to the shift towards higher Φ from the ideal curve. On the other hand, for $Q_{fnet} < 0$, $p_{I/B}$ takes the higher values compared to the ideal curve (due to attracting the free holes towards the oxide/barrier interface by the negative Q_{fnet}). As a result, for $Q_{fnet} < 0$ at a given Φ, ΔC is much higher than in ideal conditions that gives the shift towards lower Φ from the ideal curve.

In the case of Q_{it}, the mechanism of shifting the $\Delta C(\Phi)$ curves is similar like in the case of Q_{fnet}. However, the shift from the ideal curve changes with Φ due to the dependence of Q_{it} vs. Φ. In particular, for the donor-like states, Q_{it} becomes more positive with increasing Φ (due to the shifting E_{fp} towards E_V), and thus, the shift from the ideal curve increases vs. Φ. On the contrary, for the acceptor-like states, Q_{it} is less negative with increasing Φ, which leads to the reduced shift from the ideal curve with Φ. Additionally, from Fig. 5 it is evident that the $\Delta C(\Phi)$ curves are almost the same for different values of τ. This is because τ does not significantly influence p distribution in the barrier, as shown in Fig. 4, and thus, $\Delta C(\Phi)$ curves do not change for various τ.

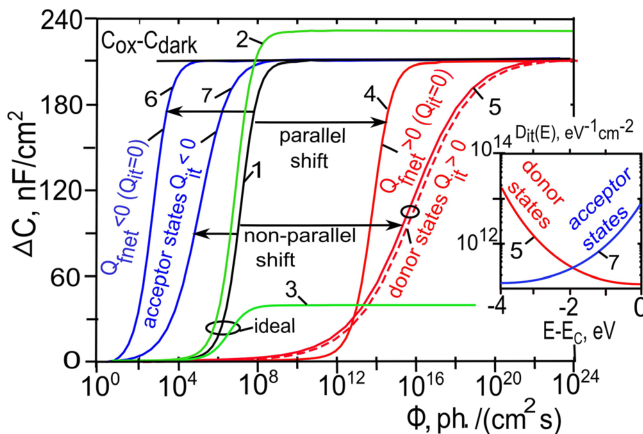

FIG. 5. $\Delta C(\Phi)$ curves calculated according to the model from Sec. IV A, for Al_2O_3/AlGaN/GaN structure under $V_G = -4$ V, in the case of an ideal Al_2O_3/AlGaN interface ($Q_{it} = 0$, $Q_{fnet} = 0$) (curves 1, 2, 3) and non-ideal interfaces with the positive $Q_{fnet} = 10^{12}$ q/cm^2 ($Q_{it} = 0$) (curve 4) with donor-like states ($Q_{it} > 0$, $Q_{fnet} = 0$) (curve 5), with the negative $Q_{fnet} = -10^{12}$ q/cm^2 ($Q_{it} = 0$) (curve 6) and with acceptor-like states ($Q_{it} < 0$, $Q_{fnet} = 0$) (curve 7). Curves 1, 4–7 calculated for $d_I = 20$ nm and $d_B = 25$ nm, curve 2 for $d_I = 20$ nm and $d_B = 35$ nm, curve 3 for $d_I = 45$ nm and $d_B = 25$ nm. Solid lines correspond to $\tau = 10^{-7}$ s and dashed line to $\tau = 10^{-9}$ s. In the inset given $D_{it}(E)$ assumed in calculations.

C. Method for determination of D_{it}(E)

In order to determine $D_{it}(E)$ near E_V, we applied the method developed by us in Ref. 19, which is based on the measurements of $\Delta C(\Phi)$ dependencies at $V_{th} < V_{G1}$. A such the V_G range is applied in order to obtain accumulation in GaN layer to avoid the uncontrolled increase of the GaN layer capacitance under illumination with $h\nu > E_G$. Furthermore, in order to enhance this approach, one should use two different biases, one close to V_{th} and the second much higher than V_{th}. This allows to extend the energy range of the scanned interface states. For example, in Ref. 19 for V_{G1} close to V_{th}, we obtained $D_{it}(E)$ distributed close to E_V, whereas for V_{G1} much higher than V_{th}, $D_{it}(E)$ was far from E_V. In our measurements of $\Delta C(\Phi)$ dependencies, we applied $V_{G1} = -2$ and -4 V for all investigated structures. The bias $V_{G1} = -4$ V was chosen as a maximum value close to V_{th}, which allowed to avoid the structure breakdown under illumination, whereas $V_{G1} = -2$ V was much higher than V_{th} and allowed to detect the lowest ΔC signal in the whole applied Φ range. The measured dependencies $\Delta C(\Phi)$ are summarized in Fig. 6.

In the first step of the method used to determine $D_{it}(E)$, we calculated the set of $\Delta C(\Phi)$ curves corresponding to the uniform distributions $D_{it}{}^{i}(E)$, which pass through all experimental points, as shown in Fig. 6(a) for two succeeding

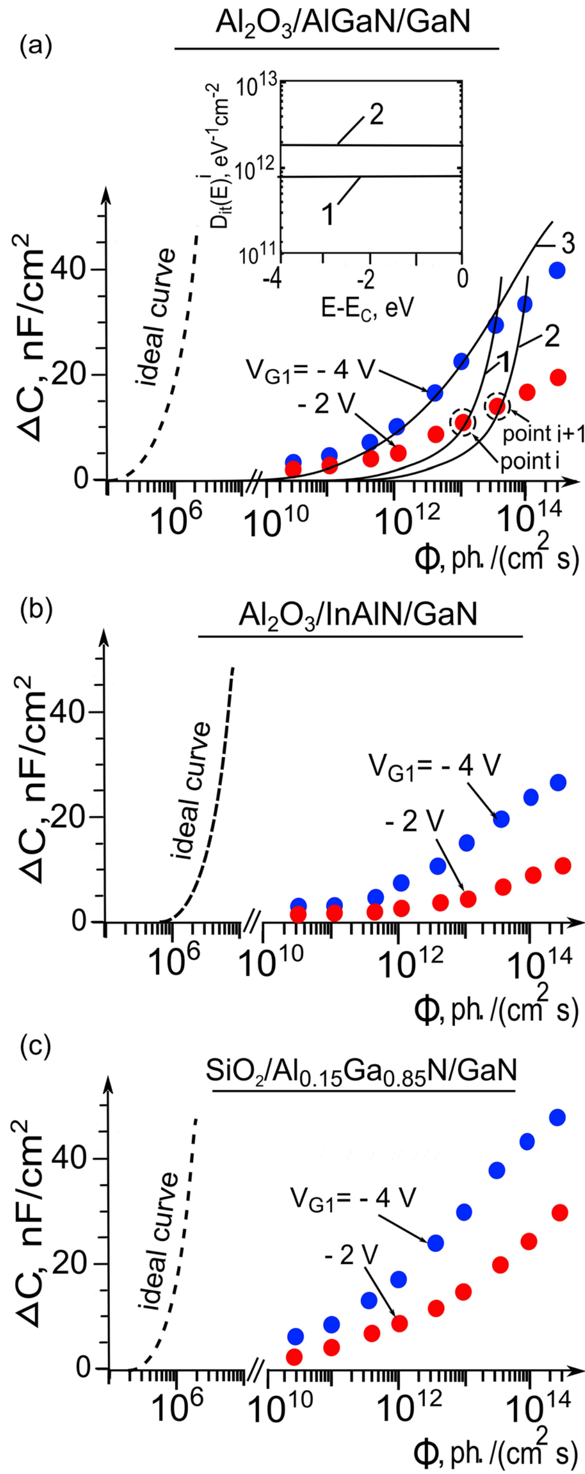

FIG. 6. Experimental dependencies of $\Delta C(\Phi)$ (points) under $V_{G1} = -2$ V and -4 V for different MISH structures at RT. Dashed lines correspond to the ideal interface ($D_{it}(E) = 0$). Solid lines 1 and 2 (a) calculated for the uniform $D_{it}{}^i(E)$ (inset) passing through the succeeding points i and i+1. Curve 3 (a) calculated for the determined U-shaped $D_{it}(E)$ and $Q_{fnet} = -10^{12}$ q/cm^2 (Sec. VIII B).

points, i and i + 1 (i = 1, 2, 3…N, where N is the number of points at the experimental $\Delta C(\Phi)$ dependence). The determined $D_{it}{}^i(E)$ allows to calculate Q^i_{it} and hole quasi-Fermi position (E^i_{fp}) at the oxide/barrier interface for the ith experimental point. On this basis, in the next step we calculated $D_{it}(E)$ using the following relationship:[19]

$$D_{it}(E) = \left| \frac{Q^{j+1}_{it} - Q^j_{it}}{E^{j+1}_{fp} - E^j_{fp}} \right|. \tag{12}$$

The obtained $D_{it}(E)$ were distributed in the energy range from near E_V to 0.5 eV above E_V, as presented in Fig. 12. It should be noted that the important advantage of the applied approach is the lack of impact of τ on the determined $D_{it}(E)$ because of independence of ΔC on τ, as it was shown in Sec. IV B. Furthermore, in Ref. 19, we proved that using this method for determination of $D_{it}(E)$ does not require the knowledge on Q_{fnet}. In order to evaluate the charge character (donor-like or acceptor-like) of the obtained $D_{it}(E)$, we compared the measured $\Delta C(\Phi)$ dependencies with the calculated ideal curve ($D_{it}(E) = 0$), as shown in Fig. 6. It is evident that all experimental $\Delta C(\Phi)$ curves are non-parallel shifted by several orders of magnitude towards higher Φ values with respect to the ideal one. This means, according to the considerations in Sec. IV B (Fig. 5) that the determined interface states are of donor-like type.

V. ESTIMATION OF D_{it} NEAR THE MIDGAP AND CONDUCTION BAND FROM $h\nu$ AND T-DEPENDENCE OF $\triangle V_{th}$

In the next step, we determined $D_{it}(E)$ from $h\nu$ and T-dependencies of $\triangle V_{th}$. In Fig. 7(a), we present the T-dependencies of $\triangle V_{th}$ obtained for $h\nu = 2$ eV. It is obvious that for all the structures the light-induced $\triangle V_{th}$ strongly decreased vs. T. As it was shown recently, this feature can be explained as follows. Due to illumination by the photons with energy $h\nu$ at a given T, the induced $\triangle V_{th}$ is equal to[29]

$$\triangle V_{th} = q \int_{E_{tm}}^{h\nu} D_{it}(E) dE / C_{total}, \tag{13}$$

where C_{total} is C_{dark} for $V_G = 0$ and the E_{tm} value is given as follows:

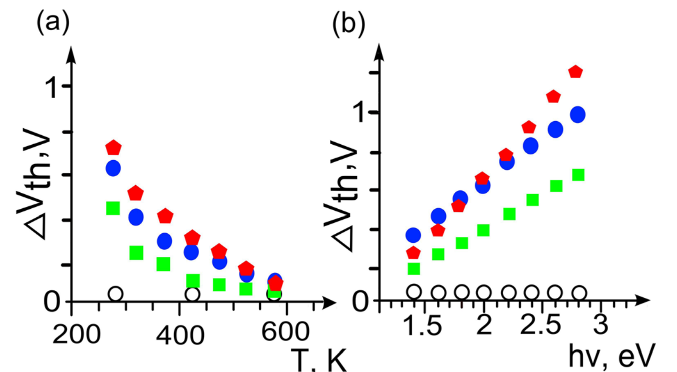

FIG. 7. Experimental dependencies of $\triangle V_{th}$ vs. T under illumination with $h\nu = 2$ eV (a) and $\triangle V_{th}$ vs. $h\nu$ at RT (full symbols) (b). Dependencies for Schottky gate structures (open circles) given for comparison.

$$E_{tm} = kT\ln(v_{th}\sigma_n N_C t_{emit}). \tag{14}$$

As it results from the above equations, due to an increase of T, E_{tm} is shifted down on the energy scale, and thus, $\triangle V_{th}$ is reduced. On the basis of Eqs. (13) and (14), we can determine $D_{it}(E)$ from the following relationship:

$$D_{it}(E) = \frac{C_{total}\left(\triangle V_{th}^{T_1} - \triangle V_{th}^{T_2}\right)}{q(E_{tm1} - E_{tm2})}, \tag{15}$$

where the E_{tm1} and E_{tm2} is E_{tm} for T_1 and T_2, respectively; $\triangle V_{th}^{T_1}$ and $\triangle V_{th}^{T_2}$ is $\triangle V_{th}$ for T_1 and T_2, respectively.

In Fig. 7(b), we present the hv-dependencies of $\triangle V_{th}$ obtained at RT. It is evident that $\triangle V_{th}$ increases vs. hv, that is caused by an increasing number of the depopulated interface states (Eq. (13)). Based on the approach proposed by Mizue *et al.*,[14] we can determine $D_{it}(E)$ from hv-dependencies of $\triangle V_{th}$ using the following formula:

$$D_{it}(E) = \frac{C_{total}\left(\triangle V_{th}^{hv_2} - \triangle V_{th}^{hv_1}\right)}{q(hv_2 - hv_1)}, \tag{16}$$

where the $\triangle V_{th}^{hv_1}$ and $\triangle V_{th}^{hv_2}$ is the value of $\triangle V_{th}$ for hv_1 and hv_2, respectively.

The estimated $D_{it}(E)$ from Eqs. (15) and (16) at the examined insulator/III-N heterojunction interfaces, which are distributed in the energy band gap between E_C and about 3 eV below E_C, are summarized in Fig. 12. Additionally, in Fig. 12(a), we also presented $D_{it}(E)$ obtained from the fitting of the C-V curve for the same Al_2O_3/AlGaN/GaN structure, as reported by Yatabe *et al.* in Ref. 13. It is clear that this $D_{it}(E)$ is consistent with $D_{it}(E)$ determined from Eq. (16), which is an independent confirmation of the reliability of the method based on the measurement of T-dependencies of $\triangle V_{th}$.

VI. ELIMINATING THE CONTRIBUTION OF BULK TRAPS AND BORDER TRAPS TO PHOTO-ELECTRICAL MEASUREMENTS

In order to eliminate the possible distorting contribution of the bulk traps located in GaN, barrier, and oxide layers, as well as of the border traps in oxide to the obtained results concerning the oxide/barrier interface states, we performed an additional study on the behaviour of photo-induced $\triangle V_{th}$ in the examined MISH structures.

A. Bulk traps in GaN and barrier layers

First, we showed that the registered $\triangle V_{th}$ is not related to the bulk traps in GaN and barrier layers. It is well known that (In, Al, Ga)N materials contain several types of electronic defect states in the bandgap. These states can be excited due to illumination/heating, and as a result, the V_{th} shift in C-V curves can be induced. Therefore, we performed the measurements of $\triangle V_{th}$ vs. hv and T for Schottky-gated structures, whose results are summarized in Fig. 7. One can note that $\triangle V_{th} \approx 0$ in the wide range of hv and T. This indicates that deep level traps in the barrier layer and/or GaN epitaxial layers have a negligible impact on the photo-assisted C-V measurements. Furthermore, it should be also noted that the bulk parameters do not markedly influence the dependencies of ΔC vs. Φ, as shown in Section IV B.

B. Bulk traps and border traps in oxides

Subsequently, we examined the possible contribution of bulk oxide traps to the photo-assisted C-V measurements. In the case where the bulk oxide traps are excited by illumination, the product $\Delta V_{th} \cdot C_{total}$ would exhibit a strong dependence on the oxide thickness. Therefore, we compared the hv dependencies of $V_{th} \cdot C_{total}$ registered for two different thicknesses of oxide layers, as shown in Fig. 8. It is evident that the hv dependencies of $V_{th} \cdot C_{total}$ are almost the same, which means that the bulk oxide traps have the negligible impact on the photo-assisted C-V measurements.

Then, an important and complex issue was to prove that the border traps do not influence $\triangle V_{th}$. This is because the border traps are located very close to the interface and they can behave like the interface states, as showed recently by Wu *et al.*[34] In order to determine if $\triangle V_{th}$ is induced by the interface states or by the border traps, we applied the following approach.

According to the band diagram shown in Fig. 9, the illumination of the structure by light with hv below the band gap of GaN, at a given T_1 and $V_{th} < V_G$, induces the depopulation of electrons from the border traps distributed between hv and E_{tm} (with respect to the oxide E_C) and from the interface states distributed (i) between hv and E_{tm} (with respect to the barrier E_C) if the interface states are not at equilibrium conditions in the dark (Fig. 9(a)) (E_{tm} is above E_f at the oxide/barrier interface) and (ii) between hv and E_{tm} if these states are at equilibrium conditions in the dark (Fig. 9(b)). Therefore, the induced $\triangle V_{th}$ can be expressed as follows:

$$\triangle V_{th} = \triangle V_{BT} + \triangle V_{IS}, \tag{17}$$

where $\triangle V_{BT}$ and $\triangle V_{IS}$ are the V_{th} shifts caused by the border traps and the interface states, respectively. These shifts are given by the following formulas, respectively:

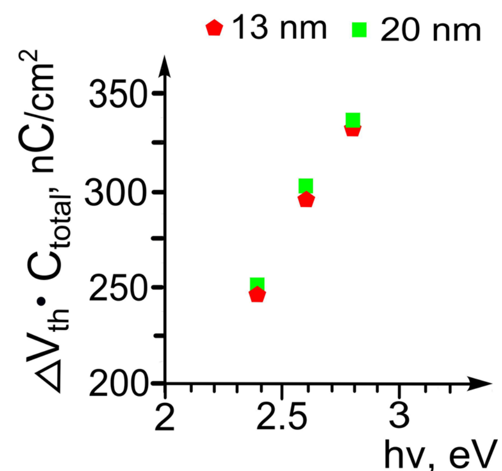

FIG. 8. Experimental dependencies of $\triangle V_{th} \cdot C_{total}$ vs. hv for Al_2O_3/InAlN/GaN structures with $d_I = 13$ nm (from Ref. 33) and $d_I = 20$ nm.

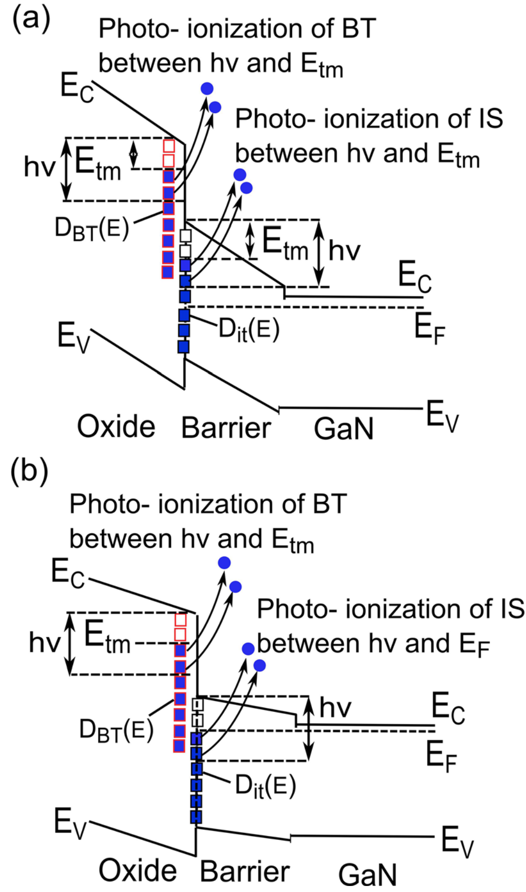

FIG. 9. Schematic band diagrams of an illuminated MISH structure (hv lower than the GaN band gap) under $V_{th} < V_G$, at T_1 with border traps and interface states at non-equilibrium (a) and at equilibrium (b). BT and IS denote the border traps and interface states, respectively.

$$\triangle V_{BT} = q \int_{E_{tm}}^{hv} D_{BT}(E) dE / C_{total}, \quad (18)$$

where $D_{BT}(E)$ is the energy distribution of the border trap density, and

(i) for the interface states under non-equilibrium in the dark:

$$\triangle V_{IS} = q \int_{E_{tm}}^{hv} D_{it}(E) dE / C_{total} \quad (19)$$

and

(ii) for the interface states under equilibrium in the dark:

$$\triangle V_{IS} = q \int_{E_C - E_f}^{hv} D_{it}(E) dE / C_{total}. \quad (20)$$

In Fig. 10(a), we displayed the calculated dependencies of E_f at the Al_2O_3/AlGaN interface vs. T, at $V_G = 1$ V and $V_G = 0$ in the dark. In the calculation, we assumed $D_{it}(E)$ (from Fig. 12(a)) and the full compensation ($Q_{fnet} = 0$). For the comparison, in Fig. 10(a) it is shown the dependence of E_{tm} vs. T calculated from Eq. (14). One can note the marked shift of E_{tm} in the bandgap, contrary to almost negligible changes of E_f. In addition, it is clear that for $V_G = 1$ V,

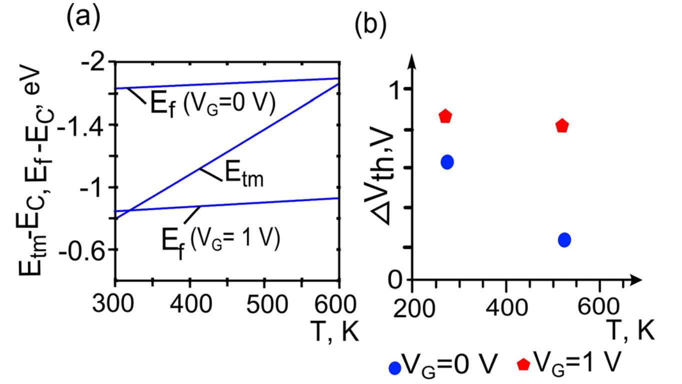

FIG. 10. Calculated dependencies of E_f at Al_2O_3/AlGaN interface vs. T, in the dark, under $V_G = 0$ V and $V_G = 1$ V, and for comparison, calculated dependence of E_{tm} vs. T (from Eq. (14)) with assumed $\sigma = 10^{-16}$ cm^{-2} (a). Measured $\triangle V_{th}$ for Al_2O_3/AlGaN/GaN structure at RT and 473 K, under $hv = 2.2$ eV for $V_G = 0$ and $V_G = 1$ V(b).

the interface states can remain at equilibrium in the wide temperature range. Therefore, it is obvious that from the measurements of $\triangle V_{th}$ performed at $V_G = 1$ V and at two different T (T_1 and $T_2 \gg T_1$) we can recognize if the border traps contribute to $\triangle V_{th}$. Namely, from Eq. (18) it is evident that $\triangle V_{BT}$ should be lower at T_2 than at T_1 due to changing E_{tm} with T (Fig. 10(a)). On the other hand, assuming that the interface states are at equilibrium at T_1 and T_2 for $V_G = 1$ V, we find from Eq. (20) that $\triangle V_{IS}$ should be the same at T_1 and T_2 due to the negligible changes of E_f vs. T (Fig. 10(a)). Therefore, if the border traps contribute to $\triangle V_{th}$, the $\triangle V_{th}$ value at T_2 should be lower than at T_1, and, on the contrary, if the border traps do not contribute to $\triangle V_{th}$, this value should remain the same at T_1 and T_2. In Fig. 10(b), we showed the measured $\triangle V_{th}$ obtained at RT and 473 K, under $hv = 2.2$ eV, for $V_G = 1$ V and $V_G = 0$ for the Al_2O_3/AlGaN/GaN structure. One can note that $\triangle V_{th}$ markedly decreased at higher T, for $V_G = 0$ V, and almost did not change for $V_G = 1$ V. Therefore, on this basis, we can neglect the contribution of the border traps to photo-assisted C-V measurements in the case of the Al_2O_3/AlGaN/GaN structure. Similar results were obtained for other MISH structures from the analogous analysis.

The reason of the lack of detection of the border traps can be either their absence ($D_{BT} = 0$) or their full depopulation of electrons (ionization) in the analyzed energy range (up to 2.2 eV, with respect to the oxide E_C). The border traps can also have the optical photoionization cross section much lower than the interface states. The latter situation means that the efficient excitation of the border traps needs illumination with stronger intensity.

Finally, we discussed the possible influence of bulk traps in oxides and the border traps on the dependencies of ΔC vs. Φ. As discussed in Sec. IV B, ΔC is determined by p at the oxide/barrier interface; therefore, the bulk and border traps in oxide would exhibit impact on ΔC vs. Φ dependencies only if the p tunneling occurs inside the oxide layer. Because the leakage currents under illumination are negligible (less than 5×10^{-8} A/cm^2), we could exclude the p tunneling into oxide, and thus, also contribution of the bulk oxide/border traps to ΔC.

VII. AES CHARACTERIZATION

After the photo-electrical characterization, we performed the AES profiling of the studied samples in order to determine the in-depth distribution of constituent elements, in particular, in the surface and interface regions. The registered AES spectra and variations of the element content versus the sputtering time for the SiO_2/AlGaN/GaN and Al_2O_3/AlGaN/GaN structures are summarized in Fig. 11. It is worth to highlight that all element peaks, i.e., C KLL, O KLL, Si KLL, Al KLL, N KLL, and Ga MNN are well resolved, and thus, based on their evolution, we could well recognize the oxide films, AlGaN barrier layer, and GaN substrate, as well as the interfacial regions (shadowed areas in Figs. 11(b) and 11(d)), i.e., the outer insulator surface, the insulator/barrier interface, and AlGaN/GaN interface. The first few AES spectra correspond to the oxide surface/subsurface regions, which are obviously non-stoichiometric with some oxygen deficiency and carbon contamination (C concentration below 20%), which totally decays at a shallow depth in both dielectric films to the AES detection level (Figs. 11(b) and 11(d)). Subsequently, with further sputtering, the concentrations of O and Si in SiO_2, and O and Al in the Al_2O_3 film become almost constant over the sputtered thickness that means the uniform and stoichiometric chemical composition of the fabricated oxide films. Then, the oxide/barrier interface region is well visible due to the correlated decay of oxide elements (O and Si in SiO_2, and O and Al in Al_2O_3 films) with gradual rising of Al, Ga, and N of the barrier layer. However, the precise determination of the transition region thickness between the oxide and AlGaN is rather difficult because of the possible ion sputtering induced artifacts, including preferential sputtering and atom mixing, which cause some widening of the interfacial region. It should be stressed that all the examined oxide layers and oxide/barrier interfaces were free of carbon contaminations. It is also evident that the element concentrations corresponding to the bulk region of AlGaN and GaN were consistent with the sample compositions.

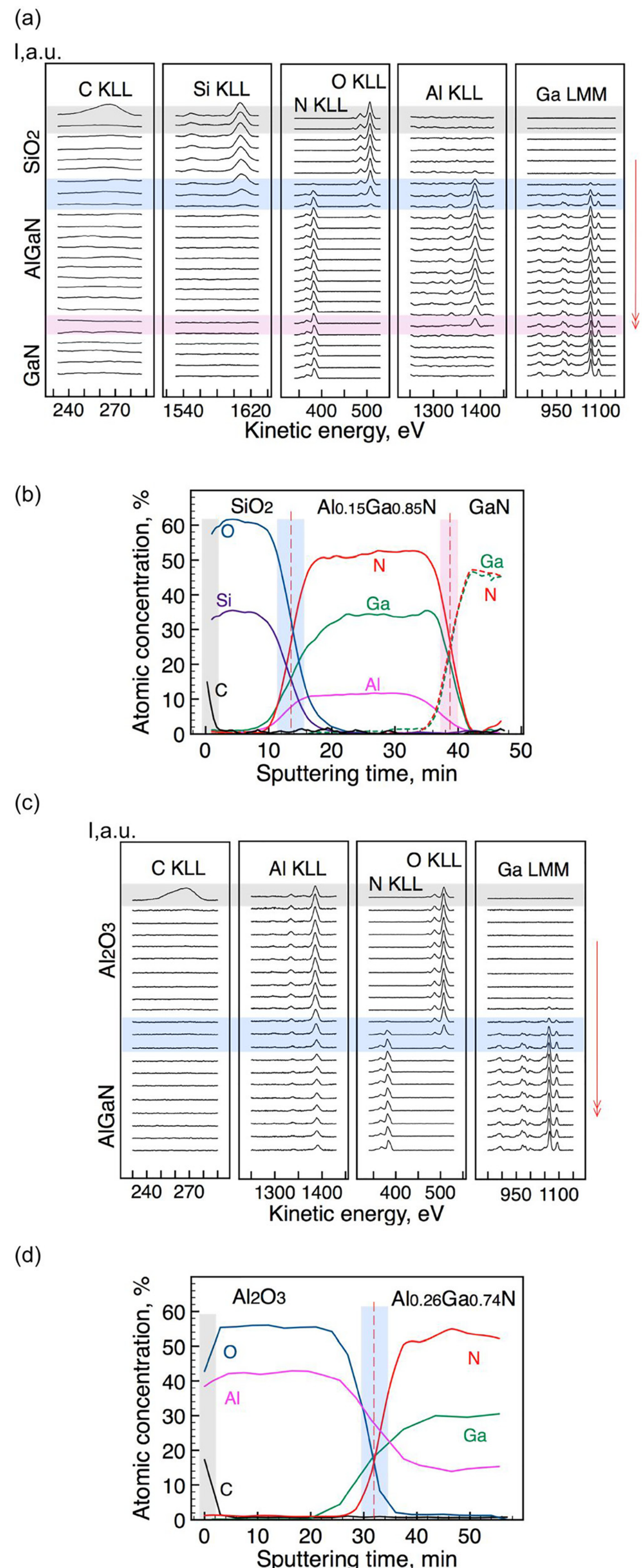

FIG. 11. Evolution of AES spectra with sputtering time and in-depth profiles of constituent element content for SiO_2/AlGaN/GaN ((a) and (b)) and Al_2O_3/AlGaN/GaN ((c) and (d)) structures, respectively.

VIII. DISCUSSION

A. Properties of D_{it}(E)

In this section, we focus on the explanation of the two following features of $D_{it}(E)$. Namely, from Fig. 12, it is evident that: (i) for all structures $D_{it}(E)$ is a typical continuous U-shaped distribution increasing towards both the CB and the VB from the midgap and (ii) $D_{it}(E)$ increases with x in the whole bandgap.

According to some reports,[35–37] the origin of interface states at oxide/III-N interfaces can be related to C impurities near/at the interface. Choi *et al.*[35] using the first principles calculations showed that C_{Al} can produce traps near/at the Al_2O_3/III-nitride interface. Based on these results as well as on the comparative electrical and photoelectric studies, Liu *et al.*[36] suggested that the slow interface states at Al_2O_3/GaN interfaces originate from C impurities. Furthermore, Jackson *et al.*[37] using the capacitance deep level optical spectroscopy claimed that $D_{it}(E)$ near VB at Al_2O_3/GaN interface is due to residual C atoms from nucleation of the ALD process. However, our AES results showed that in the investigated structures such impurities are not present in the oxide/III-N interface region at the AES detection limit (Fig. 11).

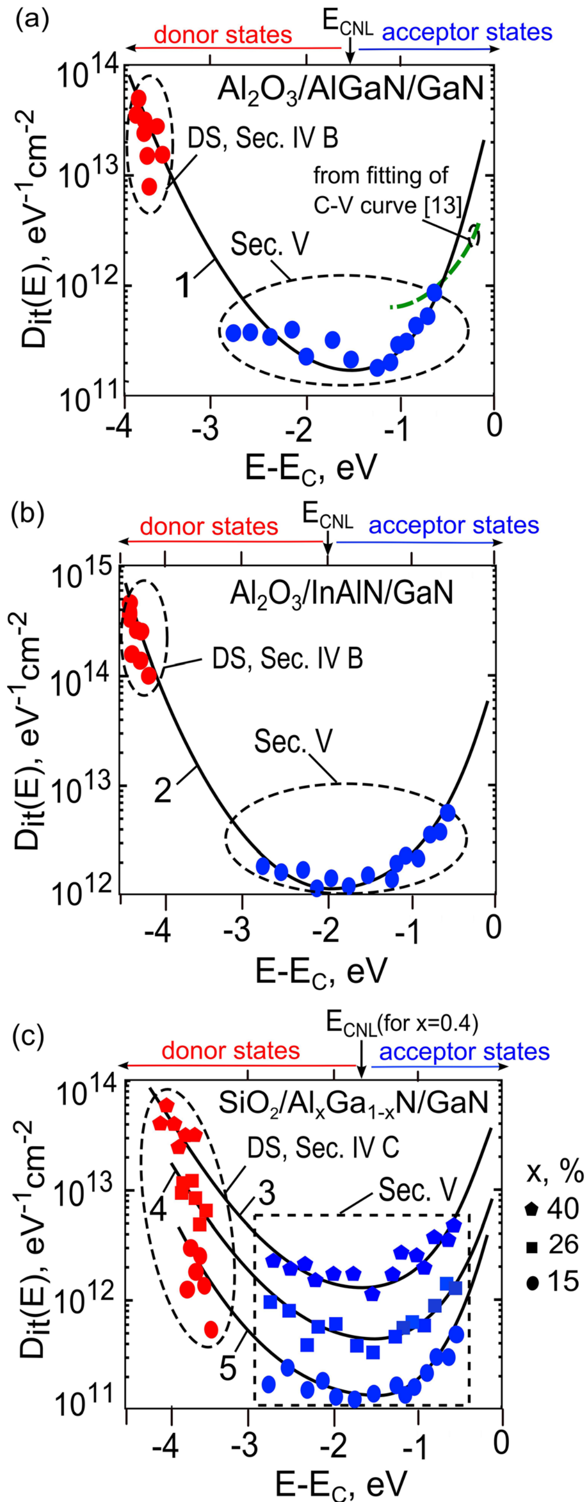

FIG. 12. $D_{it}(E)$ determined in Sec. IV C (DS means donor-like states, red points) and in Sec. V (blue points); solid lines are the best fit curves (Eq. (21)); dashed line in Fig. 12(a) is $D_{it}(E)$ from fitting of the C-V curve for the same structure as in Ref. 13. The total acceptor-like state density (D_{it}^A) and total donor-like state density (D_{it}^D) are in cm^{-2}, for curve 1: $D_{it}^A = 5 \times 10^{12}$ and $D_{it}^D = 2 \times 10^{13}$; curve 2: $D_{it}^A = 2 \times 10^{13}$ and $D_{it}^D = 3 \times 10^{14}$; curve 3: $D_{it}^A = 1.5 \times 10^{13}$ and $D_{it}^D = 4 \times 10^{13}$; curve 4: $D_{it}^A = 4 \times 10^{12}$ and $D_{it}^D = 9.5 \times 10^{12}$; and curve 5: $D_{it}^A = 2 \times 10^{12}$ and $D_{it}^D = 4 \times 10^{12}$.

Therefore, the obtained $D_{it}(E)$ (Fig. 12) cannot be explained in terms of C impurities. On the other hand, few reports suggested that the interface states at oxide/III-N interfaces originate from Ga/Al dangling bonds (DBs).[17,38] However, according to first principles calculations, Al and Ga DBs have defect energies close to CB and around the midgap.[39,40] Therefore, Ga/Al DBs can well explain only the high-density interface states near the CB but not those close to the VB.

On the contrary, the obtained U-shape of $D_{it}(E)$ can be well understood in terms of the unified disorder induced gap state model (DIGS model) proposed by Hasegawa and Ohno.[41] Within this model, the interface states are induced by the disorder of bonds near the interface produced during its formation process. The U-shaped distribution of interface states is a natural consequence of the fact that the bonding states try to minimize their energy during the interface formation. Furthermore, the DIGS model predicts that the interface states decay exponentially from CB and VB toward the midgap according to the following relationship:[41]

$$D_{it}(E) = D_{it0} \exp\left(\left|\frac{E - E_{CNL}}{E_{0d,0a}}\right|^{n_{d,a}}\right), \quad (21)$$

where D_{it0} is the minimum density, E_{0d}/E_{0a} and n_d/n_a describe the shape of the donor/acceptor branch (separated by E_{CNL}), respectively.

In Fig. 12, we showed a fit of the DIGS model expression (Eq. (21)) to the experimental spectrum $D_{it}(E)$. One can note that the obtained $D_{it}(E)$ can be well described by a theoretical dependence. This is a strong suggestion that the interface states at oxide/III-nitride interfaces can arise from the structural disorder of the interfacial region.[41] It needs to be highlighted that the DIGS model predicts the existence of donor-like interface states below E_{CNL}, which is consistent with our findings. Furthermore, the increase of $D_{it}(E)$ vs. x, according to the DIGS model, can be induced by the growing disorder with rising x that results from a gradual enhancement of strain in AlGaN films. Additionally, the DIGS model predicts that the variation of U-shaped continuum with an increasing degree of disorder should occur in the whole bang gap, i.e., for both the VB and CB side,[41] which is compatible with our observations of the $D_{it}(E)$ evolution vs. x.

B. Oxide/barrier interface charges

Recently, Bakeroot *et al.*[22] showed that for the U-shaped DIGS continuum, the equilibrium E_f at the SiN/AlGaN interface would be pinned very deeply with respect to E_{CNL}, and thus, the resulting 2DEG density would be too low. This situation, according to the cited authors, can be avoided if we assume the existence of a certain positive fixed charge at the SiN/AlGaN interface besides the U-shaped DIGS which can compensate the negative polarization charge. The authors of Ref. 22 proposed that the role of the positive fixed charge can be played by a deep border trap localized inside SiN.

In the present work, for the determined U-shaped $D_{it}(E)$ (Fig. 12) we found, from the calculations, that the equilibrium E_f position at the investigated oxide/barrier interfaces is also significantly below E_{CNL}. For example, in the case of the $Al_xGa_{1-x}N$ barrier with x of 0.2 or 0.26, for the assumed[15] $Q_{pol}^- = -9 \times 10^{12}$ q/cm^2, it was found that E_f at the $SiO_2/Al_{0.26}Ga_{0.74}N$ interface would lie at 0.74 eV below E_{CNL} and at the $Al_2O_3/Al_{0.2}Ga_{0.8}N$ interface at

1.8 eV below E_{CNL}. In the case of the $In_{0.19}Al_{0.81}N$ barrier, for the assumed[42] $Q_{pol}^{-} = -2 \times 10^{13}$ q/cm^2, it was obtained that E_f at the $Al_2O_3/In_{0.19}Al_{0.81}N$ interface would be located at 0.61 eV below E_{CNL}. As a consequence of such a low E_f position, the 2DEG density would be evidently too low.[22] Therefore, an additional positive fixed charge Q_F should be introduced at the oxide/barrier interface. Furthermore, we supported this statement by the calculations of V_{th} in C-V curves. For example, assuming the determined $D_{it}(E)$ and $Q_F = 0$ ($Q_{fnet} = Q_{pol}^{-}$), we found that V_{th} in C-V curves would be much higher (more positive) than the measured one. In particular, for the $SiO_2/Al_{0.26}Ga_{0.74}N$, $Al_2O_3/Al_{0.2}Ga_{0.8}N$, and $Al_2O_3/In_{0.19}Al_{0.81}N$ structures, we obtained $V_{th} = -4.4$ V, -5.8 V, and -6.2 V, respectively, which is completely different from that in Table I. This indicates that it is necessary to introduce the positive Q_F at the oxide/barrier interface in order to shift V_{th} towards much more negative values. From the fitting of V_{th} in the measured C-V curves, we determined Q_F for $SiO_2/Al_{0.26}Ga_{0.74}N$, $Al_2O_3/Al_{0.2}Ga_{0.8}N$, and $Al_2O_3/In_{0.19}Al_{0.81}N$ interfaces, which amounts to 8.05×10^{12} q/cm^2, 7.1×10^{12} q/cm^2, and 1.1×10^{13} q/cm^2, respectively. It should be emphasized that these values are close to Q_{pol}^{-}. We also found that the obtained Q_F corresponds to the equilibrium E_f located at 0.45 eV, 0.14 eV, and 0.24 eV above E_{CNL}, respectively. Such the position of E_f should be sufficient to obtain the suitable values of the 2DEG density.[22]

It should be noted that the net fixed charge ($Q_{fnet} = Q_{pol}^{-} + Q_F$) for these structures takes the negative values approximately equal to -10^{12} q/cm^2. According to the considerations in Sec. IV B (Fig. 5), the negative Q_{fnet} can induce a significant shift of $\Delta C(\Phi)$ curves towards much lower Φ from the ideal curve, if the positive Q_{it} under illumination is less than Q_{fnet}. The value of Q_{it} under excitation can be estimated approximately by the total density of donor states in the bandgap (because E_{fp} is close to E_V under excitation) which is in the range from 4×10^{12} to 3×10^{14} cm^{-2} for the investigated structures (see Fig. 12). Thus, the resulting shift of $\Delta C(\Phi)$ curves from the ideal one should be in the direction of much higher Φ, which is in accordance with our observations (Fig. 6). In order to quantitatively confirm this shift, we calculated the $\Delta C(\Phi)$ dependence for $Al_2O_3/Al_{0.2}Ga_{0.8}N$ at $V_{G1} = -4$ V with the assumption of the determined Q_{fnet}, $D_{it}(E)$ (approximated by exponential curves, according to Eq. (21)) and $Q_{pol}^{-} = -9 \times 10^{12}\, q/\mathrm{cm}^2$. We obtained, as shown in Fig. 6(a) (curve 3), a very good approximation of the experimental $\Delta C(\Phi)$ dependence by the simulated curve, which additionally supports the validity of the independently estimated Q_{fnet} and $D_{it}(E)$ magnitudes. However, further studies are necessary to better understand the origin of the relevant fixed charges at oxide/III-nitride heterojunction interfaces.

IX. CONCLUSIONS

In conclusion, we determined the $D_{it}(E)$ spectrum of interface states at Al_2O_3/AlGaN, $SiO_2/Al_xGa_{1-x}N$, and Al_2O_3/InAlN interfaces in the entire bandgap, in particular, near the VB, using the photo-assisted C-V and photo-capacitance methods. In general, for all examined structures we found that: (*i*) $D_{it}(E)$ is a continuous U-shaped distribution increasing towards both CB and VB from the midgap and (*ii*) interface states near the VB exhibited donor-like character. Furthermore, we revealed that $D_{it}(E)$ for SiO_2/Al_xGa_{1-x}/GaN structure increases with increasing x. In order to identify C impurities, which can be responsible for $D_{it}(E)$, we characterized the chemical composition of the interface region by means of AES profiling. We showed, at the AES detection limit, that such impurities are not present in the oxide/III-N interface region, which indicates that $D_{it}(E)$ is not related to carbon as it was previously claimed. Finally, we proved that the determined U-shaped $D_{it}(E)$ spectrum can be well fitted using a formula predicted by the DIGS model. This finding indicates that the interface states at oxide/III-N interfaces probably originate from the structural disorder of the interfacial region. We also revealed at the oxide/barrier interfaces the presence of the positive fixed charge, which is not related to $D_{it}(E)$ and which almost compensates the negative polarization charge.

ACKNOWLEDGMENTS

This work was partially supported by the National Science Center in Poland within the project No. NCN 515 606 339 and the Visegrad Group (V4)-Japan Joint Research Program, the project entitled "Highly Safe GaN Metal-Oxide-Semiconductor Transistor Switch" (SAFEMOST); No. 14/990/PNN16/0072 by the National Centre for Research and Development (CNBR) in Poland.

[1]U. K. Mishra, L. Shen, T. E. Kazior, and Y. F. Wu, Proc. IEEE **96**, 287 (2008).
[2]J. Kuzmik, IEEE Electron Device Lett. **22**, 510 (2001).
[3]Z. Yatabe, J. Asubar, and T. Hashizume, J. Phys. D: Appl. Phys. **49**, 393001 (2016).
[4]M. Kanamura, T. Ohki, T. Kikkawa, K. Imanishi, T. Imada, A. Yamada, and N. Hara, IEEE Electron Device Lett. **31**, 189 (2010).
[5]K. Shinohara, D. Regan, Y. Tang, A. Corrion, D. Brown, J. Wong, J. Robinson, H. Fung, A. Schmitz, T. Oh, S. Kim, P. Chen, R. Nagele, A. Margomenos, and M. Micovic, IEEE Trans. Electron. Devices **60**, 2982 (2013).
[6]D. S. Lee, Z. Liu, and T. Palacios, Jpn. J. Appl. Phys., Part 1 **53**, 100212 (2014).
[7]T. Ueda, M. Ishida, T. Tanaka, and D. Ueda, Jpn. J. Appl. Phys., Part 1 **53**, 100214 (2014).
[8]M. Wang, Y. Wang, C. Zhang, B. Xie, C. P. Wen, J. Wang, Y. Hao, W. Wu, K. J. Chen, and B. Shen, IEEE Trans Electron Devices **61**, 2035 (2014).
[9]T. Hashizume, S. Ootomo, T. Inagaki, and H. Hasegawa, J. Vac. Sci. Technol. B **21**, 1828 (2003).
[10]T. Hashizume, S. Ootomo, and H. Hasegawa, Appl. Phys. Lett. **83**, 2952 (2003).
[11]Y. Hori, Z. Yatabe, and T. Hashizume, J. Appl. Phys., Part 1 **114**, 244503 (2013).
[12]D. Gregusova, R. Stoklas, C. Mizue, Y. Hori, J. Novak, T. Hashizume, and P. Kordos, J. Appl. Phys. **107**, 106104 (2010).
[13]Z. Yatabe, Y. Hori, W. C. Ma, J. T. Asubar, M. Akazawa, T. Sato, and T. Hashizume, Jpn. J. Appl. Phys., Part 1 **53**, 100213 (2014).
[14]C. Mizue, Y. Hori, M. Miczek, and T. Hashizume, Jpn. J. Appl. Phys., Part 1 **50**, 021001 (2011).
[15]M. Miczek, C. Mizue, T. Hashizume, and B. Adamowicz, J. Appl. Phys. **103**, 104510 (2008).
[16]M. Tapajna and J. Kuzmik, Appl. Phys. Lett. **100**, 113509 (2012).
[17]R. D. Long, C. M. Jackson, J. Yang, A. Hazeghi, C. Hitzman, S. Majety, A. R. Arehart, Y. Nishi, T. P. Ma, S. A. Ringel, and P. C. McIntyre, Appl. Phys. Lett. **103**, 201607 (2013).
[18]M. Matys, B. Adamowicz, and T. Hashizume, Appl. Phys. Lett. **101**, 231608 (2012).

[19]M. Matys, B. Adamowicz, Y. Hori, and T. Hashizume, Appl. Phys. Lett. **103**, 021603 (2013).
[20]D. Bisi, M. Meneghini, M. Van Hove, D. Marcon, S. Stoffels, T. Wu, S. Decoutere, G. Meneghesso, and E. Zanoni, Phys. Status Solidi A **212**, 1122 (2015).
[21]P. Kordos, R. Stoklas, D. Gregusova, and J. Novak, Appl. Phys. Lett. **94**, 223512 (2009).
[22]B. Bakeroot, S. You, T.-L. Wu, J. Hu, M. Van Hove, B. De Jaeger, K. Geens, S. Stoffels, and S. Decoutere, Appl. Phys. **116**, 134506 (2014).
[23]J. Osvald, R. Stoklas, and P. Kordos, Phys. Status Solidi B **252**(5), 996–1000 (2015).
[24]Z. Yatabe, J. T. Asubar, T. Sato, and T. Hashizume, Phys. Status Solidi A **212**, 1075 (2015).
[25]Y. Hori, C. Mizue, and T. Hashizume, Jpn. J. Appl. Phys., Part 1 **49**, 080201 (2010).
[26]M. Akazawa, M. Chiba, and T. Nakano, Appl. Phys. Lett. **102**, 231605 (2013).
[27]M. Akazawa, B. Gao, T. Hashizume, M. Hiroki, S. Yamahata, and N. Shigekawa, J. Appl. Phys. **109**, 013703 (2011).
[28]M. Akazawa, T. Matsuyama, T. Hashizume, M. Hiroki, S. Yamahata, and N. Shigekawa, Appl. Phys. Lett. **96**, 132104 (2010).
[29]M. Matys, R. Stoklas, J. Kuzmik, B. Adamowicz, Z. Yatabe, and T. Hashizume, J. Appl. Phys. **119**, 205304 (2016).
[30]W. Shockley and W. T. Read, Phys. Rev. **87**, 835 (1952).
[31]H. Morkoc, *Handbook on Nitride Semiconductors and Devices*, Vol. 3: GaN-based optical and electronic devices (Wiley, Weinheim, 2009).
[32]H. Hasegawa, T. Inagaki, S. Ootomo, and T. Hashizume, J. Vac. Sci. Technol. B **21**, 1844 (2003).
[33]M. Akazawa, Jpn. J. Appl. Phys., Part 1 **53**, 028003 (2014).
[34]T.-L. Wu, J. Franco, D. Marcon, B. De Jaeger, B. Bakeroot, S. Stoffels, M. Van Hove, G. Groeseneken, and S. Decoutere, IEEE Trans. Electron Devices **63**, 1853 (2016).
[35]M. Choi, J. L. Lyons, A. Janotti, and C. G. Van de Walle, Appl. Phys. Lett. **102**, 142902 (2013).
[36]X. Liu, J. Kim, R. Yeluri, S. Lal, H. Li, J. Lu, S. Keller, B. Mazumder, J. Speck, and U. Mishra, J. Appl. Phys. **114**, 164507 (2013).
[37]C. M. Jackson, A. R. Arehart, E. Cinkilic, B. McSkimming, J. S. Speck, and S. A. Ringel, J. Appl. Phys. **113**, 204505 (2013).
[38]R. D. Long and P. C. McIntyre, Materials **5**, 1297 (2012).
[39]Ch. G. Van de Walle and D. Segev, J. Appl. Phys. **101**, 081704 (2007).
[40]M. S. Miao, A. Janotti, and C. G. Van de Walle, Phys. Rev. B **80**, 155319 (2009).
[41]H. Hasegawa and H. Ohno, J. Vac. Sci. Technol. B **4**, 1130 (1986).
[42]Z. Hu, Y. Yue, M. Zhu, B. Song, S. Gangluly, J. Bergman *et al.*, Appl. Phys. Express **7**, 031002 (2014).